J Solid State Electrochem (2016) 20:3383–3391
DOI 10.1007/s10008-016-3311-7

ORIGINAL PAPER

Pulsed electrochemical deposition of nickel oxides on multi-walled carbon nanotubes from EDTA alkaline solutions: a SEM, XPS, and voltammetric characterization

Daniele Gioia[1] · **Alessandro Laurita**[1] · **Gerardo Di Bello**[2] · **Innocenzo G. Casella**[1]

Received: 15 February 2016 / Revised: 8 June 2016 / Accepted: 28 June 2016 / Published online: 5 July 2016

Abstract A study regarding the electrodeposition of nickel oxide particles on the activated multi-walled carbon nanotubes from 2 M NaOH solution containing $Ni(NO_3)_2$ and EDTA was carried out. The electrodeposition process was carried out using an optimized double-pulse sequence of potentials: $E_1 = -0.2$ V vs. SCE ($t_1 = 0.3$ s) and $E_2 = 0.7$ V vs. SCE ($t_2 = 0.03$ s). Spectroscopic XPS investigations and SEM analysis were used in order to characterize the surface and morphology of the studied modified electrode. Cyclic voltammetry and chronoamperometry were used in order to evaluate the electrochemical/amperometric performance of the GC/MWCNT-Ni electrode toward the oxidation of some aliphatic alcohols in strong alkaline medium.

Keywords MWCNTs · Nickel · Pulsed deposition · SEM · XPS · Alkaline · Alcohols · Oxidation

Introduction

The deposition processes of single or mixing metals are of great interest and importance in the various fields of the material sciences such as electronics industries, corrosion protective coatings, energy storage and conversion devices, magnetic recording supports, water electrolysis, electrocatalytic systems, etc. [1, 2]. In particular, nanoparticles of materials based on metal species, having a high surface area, exhibit unique features such as improved magnetic and electric properties, high reactivity and enhanced catalytic activities. As a consequence, these materials have been extensively studied and proposed in various technological applications [3, 4]. These materials are expected to show advantages for use as electrode materials, in order to prevent aggregation between surface particles. Thus, among the nanoparticle species, metals or their oxides are objects of great interest in modern electrochemistry. In this respect, of all the transition metals, nickel and its oxides can be considered versatile and active electrode materials for electrochemical capacitors [5, 6], alkaline rechargeable batteries [7–11], fuel cell devices [12–15], electrochemical sensors for analytical applications [16–20], etc. In particular, in our previous investigations [21–24], we have studied chemically modified electrodes (CMEs) based on the nickel nanoparticles and successfully proposed them as sensing probes in liquid chromatography and flow injection analysis (FIA) for the detection of alcohols, amines, carbohydrates, amino acids, etc.

Generally, metal oxide coatings are electrodeposited from cyanide alkaline baths, which produce high-quality deposits with improved mechanical, electrical, and electrochemical properties [1, 2]. However, these electroplating solutions causing environmental damages require delicate manipulation in the use and disposal of cyanides. Thus, the development of electrodeposition procedures of metal oxide coatings from cyanide-free alkaline baths is of important environmental, technological, and economical interest.

Hybrid materials based on transition metals or semiconductor nanoparticles dispersed on surface-functionalized carbon nanotubes (CNTs) are one of the most actively pursued research areas. CNTs as a new allotropic form of carbon, with hexagonal honeycomb lattices, show special electronic and

Dedication in memory of Pier Giorgio Zambonin

✉ Innocenzo G. Casella
innocenzo.casella@unibas.it

[1] Dipartimento di Scienze dell'Università degli Studi della Basilicata, Via dell'Ateneo Lucano 10, 85100 Potenza, Italy

[2] Scuola di Ingegneria dell'Università degli Studi della Basilicata, Via dell'Ateneo Lucano 10, 85100 Potenza, Italy

mechanical properties. These materials have closed topology and tubular structure, with several nanometers in diameter and many microns in length. Depending on their atomic structure, CNTs behave electrically as conducting metals or as semiconductor materials. It is expected that composite electrodes made of CNTs and metal oxide nanoparticles may have improved electrode activity compared with their individual counterparts [25, 26]. Thus, highly electroactive CMEs based on CNT-Ni were recently proposed as sensing probes in several electroanalytical applications [27–29]. On the other hand, multiwalled carbon nanotubes (MWCNTs) consisting of multiple rolled layers of graphene exhibit some advantages over single-walled CNTs, such as ease of mass production, low product cost per unit, and enhanced thermal and chemical stability.

In continuation of our previous investigations in the field of surface modification of traditional electrode substrates with metal species, through the use of electrodeposition techniques, we consider in this study the preparation and characterization of a CME containing activated MWCNTs and nickel oxide species (GC/MWCNT-Ni). In particular, a pulsed electrochemical procedure of the nickel oxide deposition from alkaline solutions using a stable and nontoxic complexing ligand such as ethylene-diaminetetraacetate disodium salt (EDTA) was defined and optimized. The advantage of using EDTA as a complexing agent in electrodeposition baths for production, for example, of metallic alloys or oxide coatings is that this compound acts as a strong complexing agent in alkaline media. The prepared GC/MWCNT-Ni electrode was characterized by electrochemical, X-ray photoelectron spectroscopy (XPS) and surface electron microscopy (SEM) before and after electrochemical treatment in alkaline medium. The electrocatalytic properties of the MWCNT-Ni electrodes were tested toward the electrooxidation of some aliphatic alcohols.

Experimental

Reagents

The stock solutions were prepared by using ultrapure water supplied by a Millipore Direct-Q UV unit (Bedford, MA, USA). The used chemicals K_2SO_4, methanol, ethanol, propanol, butanol, NaOH pellets (≥98 %), and MWCNTs (>99 %) were purchased from Aldrich Chemie. All chemicals employed were of ACS grade and were used without further purification. Stock solutions of alcohols were prepared weekly in ultrapure water and stored at ambient temperature.

Apparatus

The voltammetric experiments were performed with an Autolab PGSTAT 30 Potentiostat/Galvanostat (Eco Chemie, Utrecht, The Netherlands), and the data were acquired using an Autolab GPES software package version 4.9. A SCE reference electrode and a platinum foil counter electrode used in electrochemical measurements were purchased from Amel (Milan, Italy). The glassy carbon (GC) electrodes (3-mm diameter) used as substrate electrode material were also purchased from Amel. All current densities in this paper were quoted in terms of mA cm^{-2} of apparent geometric area of substrate electrode. The experiments were carried out at ambient temperature (generally comprised between 20 and 22 °C). When necessary, the solutions were deaerated by bubbling with nitrogen prior to the electrochemical experiments.

X-ray photoelectron spectra were collected using a Leybold LH X1 spectrometer using unmonochromatized Al Kα radiation (1486.6 eV). The source was set at 15 kV and 20 mA. The binding energy (BE) scale was calibrated with respect to the Cu $2p_{3/2}$ (932.7 eV, with a full width at half maximum (FWHM) of 1.75 eV) and Au $4f_{7/2}$ (84.0 eV with a FWHM of 1.20 eV) signals. Spectra were recorded only after the wide scan showed that no features arose from the sample rod. Wide and detailed spectra were collected in fixed analyzer transmission (FAT) mode, using a pass energy of 50 eV and a channel width of 1.0 and 0.1 eV, respectively. BE values in all the figures were not corrected for surface charging, but peak positions reported in the text were adequately corrected by referring to the graphitic C1s peak after setting its BE to 284.6 eV. The vacuum in the analysis chamber was always better than 5×10^{-9} mbar. All samples before XPS analysis were washed thoroughly with ultrapure water and dried in oven.

SEM micrographs were obtained from an environmental scanning electron microscope Philips ESEM XL 30. All samples after the preparation or the electrochemical treatment were washed thoroughly with ultrapure water and dried before executing the morphological analysis.

Electrode preparation

The MWCNTs used in this study were synthesized by an electrical arc discharge method, having approximately 5–20 graphitic layers with an outer diameter of 7–15 nm and a length comprised between 0.5 and 10 μm. MWCNTs (10 mg) were dispersed in 5 mL of ultrapure water and sonicated for 60 min at room temperature. Before modification, the GC electrodes were polished with 0.05 μm α-alumina suspension on a micro-cloth polishing pad, washed with HCl (15 %), and finally treated with ultrapure water to remove traces of surface impurities. Immediately afterwards, 15 μL of MWCNT (2 mg mL^{-1}) dispersion in water was placed directly onto the GC surface (3-mm diameter). The relevant electrode containing the emulsion was allowed to dry in an oven at about 70 °C for 15 min and then rinsed with ultrapure water in order to form the GC/MWCNT substrate. The resulting electrode was cycled between −0.4 and 1.8 V vs. SCE

(40 cycles) in 0.5 M K_2SO_4 solution in order to produce surface oxide functional groups such as carbonyl, hydroxyl, and carboxyl [30, 31]. The oxygen-containing surface groups on the MWCNTs can be useful for further surface modification processes regarding the metal oxide deposition [32]. The nickel electrodeposition on the activated GC/MWCNT electrode was performed using an optimized double-pulse sequence of potentials based on the following waveform: $E_1 = -0.2$ V vs. SCE ($t_1 = 0.3$ s) and $E_2 = 0.7$ V vs. SCE ($t_2 = 0.03$ s). The total time of the nickel electrodeposition process was set at 100 s. The nickel deposition was carried out by using 2 M NaOH solution after addition of 5.0 mM EDTA and 5.0 mM $Ni(NO_3)_2$.

The apparent active surface concentration of electrodeposited nickel species (Γ_{Ni}) was evaluated by electrochemical analysis. Assuming that all nickel surface particles are electroactive on the voltammetric time scale, the Γ_{Ni} was determined by evaluating the charge (Q) under the anodic wave I_a (corresponding to the Ni(II)/Ni(III) transition), when the GC/MWCNT-Ni electrode was cycled (50 mV s^{-1}) in 1 M NaOH. The Γ_{Ni} was calculated using the Faraday equation: $\Gamma_{Ni} = Q/(nFA)$, where n is assumed to be equal to 1 and A represents the geometric area of the electrode (0.07 cm^2). A nominal surface concentration of Ni species on the GC/MWCNT-Ni electrode, comprised between 16 and 20 nmol cm^{-2}, was evaluated. The deposition efficiency or the rate of nickel oxide/hydroxide electrodeposition was expressed as a function of the amount of the nominal surface concentration of Ni oxide species (Γ_{Ni}) on the electrode substrate.

Results and discussion

Electrodeposition of nickel oxides on the activated GC/MWCNT electrode

Figure 1 compares the voltammetric profiles of the nickel species deposited on the activated GC and activated GC/MWCNT electrode substrate. The surface modification of electrode substrates with nickel species was performed by pulsed electrodeposition technique using the optimized procedure as described in the "Experimental" section. As can be seen, the modified electrodes show the typical voltammogram profiles of surfaces containing Ni(II,III) species. On the contrary, no appreciable nickel film formation was observed on the non-activated GC/MWCNT substrate (not shown here) even after significant prolonged electrodeposition times (i.e., 300 s). The nickel oxide particles deposited on the activated GC/MWCNT substrate produce stable voltammetric profiles by cycling the potentials in 1 M NaOH solution. Repetitive cyclic voltammograms were done to determine the electrochemical stability of the electrode; after the first 200 cycles,

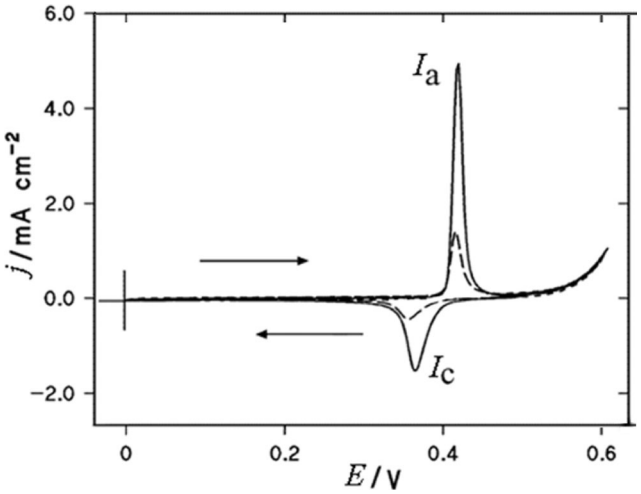

Fig. 1 Voltammograms (fifth cycle) of the nickel species deposited on the activated GC/MWCNT electrode substrate (*solid curve*) and on the activated GC electrode (*dotted curve*) in 1 M NaOH not deaerated solution at 50 mV s^{-1}. The electrochemical activation of the electrode substrate and the nickel deposition were carried out as reported in the "Electrode preparation" section

a maximum 10 % decrease of the redox peaks was generally observed. We speculated that the electrochemical activation process of the GC/MWCNT substrate in 0.5 M K_2SO_4 solution can induce a physical stabilization of nickel particles and MWCNT structures on the GC surface, due to polar interactions between the oxidized functional groups formed on the nanotubes and GC surfaces (*vide infra*).

The main electrochemical characteristics of the modified electrodes containing nickel oxides include a well-defined irreversible cathanodic wave, indicated as I_a/I_c and centered between 0.3 and 0.5 V vs. SCE, which is attributed to the Ni(II)-Ni(III) redox transition [5, 16, 17, 20–29]. The complex redox processes involving anhydrous β-$Ni(OH)_2$, hydrated α-$Ni(OH)_2$, and oxidized phases β-NiOOH and/or γ-NiOOH can coexist during continuous cycling polarization in alkaline medium [33–35]. On the basis of these experiments, it is clear that the electrochemical activation procedure of the MWCNTs plays an essential role on the overall nickel electrodeposition process (*vide infra*). Moreover, it is interesting to observe that the Γ_{Ni} is significantly affected by the presence of the nanotubes on the GC electrode surfaces. In fact, the Γ_{Ni} changes from 4.5 nmol cm^{-2} (i.e., 30 μC) to 16.5 nmol cm^{-2} (i.e., 112 μC), when GC/MWCNTs are used as electrode substrate instead of GC. Thus, the presence of the nanotube on the electrode surface produces an approximately 260 % increase in the nickel redox signals. In our opinion, this result can also be attributed to the high dispersion of the Ni species within the MWCNT structure. In this scenario, a favorable three-dimensional (3D) distribution of the catalyst particles may occur, leading to a subsequent increase of the surface roughness.

In order to define the optimal experimental conditions of the nickel electrodeposition on the activated GC/MWCNTs, the effects of the hydroxide concentration [OH^-], ligand concentration [EDTA], and pulsed waveform (i.e., applied potentials and pulse duration) were evaluated. The effects of [OH^-] and [EDTA]/[Ni(II)] concentration ratio on the efficiency of the nickel electrodeposition process are given in Table 1. In the first instance, the [OH^-] has a significant influence on the rate of nickel oxide deposition; using a solution with a constant [EDTA]/[Ni(II)] ratio equal to 1, while increasing the [OH^-] from 0.5 to 2.0 M, the nickel surface concentration increased from 0.07 to 17.8 nmol cm^{-2}, exhibiting an increase of approximately 250 times. For solutions containing [OH^-] equal to 0.2 M and [EDTA]/[Ni(II)] ratio equal to 1, no appreciable deposition of nickel film was observed. This behavior suggests an involvement of OH^- ions in the nickel deposition. In addition (see Table 1), the kinetics of the nickel deposition decreases markedly with increasing the [EDTA]/[Ni(II)] concentration ratio; in fact, no appreciable film formation was observed even after prolonged electrodeposition (i.e., 300 s) for [EDTA]/[Ni(II)] concentration ratio equal to 1.4 (i.e., [EDTA]/[Ni(II)] = 7/5). On the other hand, alkaline bath solutions with [EDTA]/[Ni(II)] ratio <1 are unstable, and consequently, a precipitation phenomenon of nickel hydroxide was observed. Similar effects of the [OH^-] and [EDTA]/[Ni(II)] concentration ratio on the kinetics of the nickel electrodeposition from alkaline solutions were already observed and critically discussed [36].

Table 2 summarizes the effects of the applied potential limits on the electrodeposition efficiency of the nickel on the activated MWCNTs. As can be seen from Table 2, the rate of nickel deposition decreases markedly by reducing the potential values of the anodic pulses (i.e., E_2), while the potentials of the cathodic pulse (i.e., E_1) show a maximum efficiency of nickel deposition for $E_1 = -0.2$ V vs. SCE. For applied pulses higher or lower than −0.2 V, the kinetics of the nickel electrodeposition process exhibits a decrease. Thus, a sequence of potential pulses of $E_1 = -0.2$ and $E_2 = 0.7$ V vs. SCE triggers the favorable electrodeposition of nickel from alkaline solutions containing Ni-EDTA complexes. The anodic potential (E_2) ≤0.7 V greatly minimizes the oxygen evolution process from the electrode avoiding the formation of films with cavities and pores randomly distributed on the electrode surface [5, 21, 36, 37].

Table 1 Effect of the composition of the depositing solution on the rate of the nickel electrodeposition

[OH^-] (M)	[EDTA]/[Ni(II)]	Charge of peak I_a (C)	(Γ_{Ni}, nmol cm^{-2})
1.0	6/5	6.5×10^{-6}	0.96
0.5	5/5	4.7×10^{-7}	0.07
0.2	5/5	No dep.	–
1.0	7/5	No dep.	–
2.0	5/5	1.2×10^{-4}	17.8
1.0	5/5	8.2×10^{-5}	12.1

The nickel was deposited on the activated GC/MWCNT electrode using the following double-pulse sequence of potentials: $E_1 = -0.2$ V vs. SCE (0.3 s) and $E_2 = 0.7$ V vs. SCE (0.03 s) for the total electrodeposition time of 100 s. The apparent active surface loading of the electrodeposited nickel (Γ_{Ni}, nmol cm^{-2}) was evaluated under cyclic voltammetry in 1.0 M NaOH solution at 50 mV s^{-1} by integrating the anodic wave I_a

Table 2 Effect of the pulse potentials on the rate of the nickel deposition

Potentials (E_1/E_2, V vs. SCE)	Charge of peak I_a (C)	(Γ_{Ni}, nmol cm^{-2})
−0.2 /0.9	1.8×10^{-4}	26.6
−0.2/0.7	1.26×10^{-4}	17.8
−0.2/0.5	9.8×10^{-5}	14.5
−0.2/0.3	5.8×10^{-5}	8.6
−0.4/0.7	1.1×10^{-4}	16.3
−0.6/0.7	2.6×10^{-5}	3.8
0.1/0.7	2.0×10^{-5}	2.9

The nickel was deposited on the activated GC/MWCNT electrode using a depositing solution containing 2.0 M NaOH plus 5 mM $Ni(NO_3)_2$ and 5.0 mM EDTA. The relevant times of the applied potentials were 0.3 and 0.03 s for E_1 and E_2, respectively. The apparent active surface loading of the electrodeposited nickel (Γ_{Ni}, nmol cm^{-2}) was evaluated under cyclic voltammetry in 1.0 M NaOH solution at 50 mV s^{-1} by integrating the anodic wave I_a

On the basis of our experimental data, a complex multistep mechanism involving a preliminary adsorption step of the $(Ni\text{-}EDTA)_{ads}$ complex on the activated MWCNT structures may be invoked. The application of anodic pulse potentials (E_2) positively affects the oxidation of the EDTA ligand with subsequent destruction of the adsorbed $(Ni\text{-}EDTA)_{ads}$ complex and precipitation of insoluble nickel oxide on the electrode surface. As a consequence, the rate of nickel deposition decreases sensibly by reducing the anodic excursions of the pulse potentials (E_2). Although the pulse potential E_1 plays an important role on the overall deposition process of nickel species, its interpretation appears very complex and at this time, it is not easy to explain. These experimental results suggest that in the E_1 region of potentials, various simultaneous reactions may take place on the electrode such as (i) formation of the $MWCNT(Ni\text{-}EDTA)_{ads}$ species and (ii) formation of reduced nickel metal (Ni^0), NiOH, and/or NiH species [38]. At this time, we are not able to distinguish the real contribution of each of the previous hypothesized contributions on the growth of the nickel deposit and further studies are necessary in order to rationalize the electrodeposition mechanism of nickel species on the activated MWCNTs. Nevertheless, it is clear that a continuous sequence of anodic/cathodic (E_1/E_2) pulse potentials fixed at −0.2 and at 0.7 V triggers the

favorable kinetics of the nickel electrodeposition on the activated MWCNTs.

SEM investigation of the electrodeposited nickel oxides on the activated GC/MWCNT

A morphological investigation of the GC/MWCNT-Ni-modified electrode was carried out by SEM. Figure 2a shows the surface morphology of the GC/MWCNT-Ni. The electrode shows a distribution of the material in cluster structures, due to poor dispersion capacity of the MWCNTs onto the GC. Nevertheless, the fiber-like 3D surface distribution of the MWCNTs onto the GC substrate appears prominently. Figure 2b shows a detailed picture (×9000) of the GC/MWCNT-Ni electrode surface. As can be seen from Fig. 2b, the MWCNTs appear generally as bundles with diameters ranging between 200 and 300 nm, while some agglomerates with size up to about 1 μm can clearly be seen, and their defined structures became indiscernible under SEM analysis. The length of the dispersed MWCNTs could not be measured since their ends were not both visible simultaneously. SEM images of MWCNT structures before and after pulsed electrochemical deposition of nickel particles show no appreciable morphological differences. The detailed SEM picture confirms the practical absence of agglomerate structures of nickel deposit on the outer surface of the MWCNT bundles. This result suggests that nickel oxides can be preferentially deposited inside multi-walled carbon nanotubes. Nevertheless, further investigations are necessary in order to define the morphological dispersion of the nickel particles onto the GC/MWCNT surface. On the other hand, similar results have also been observed for the modified electrodes based on Ni and Pd particles which seem introduced inside the MWCNT cavities [39, 40].

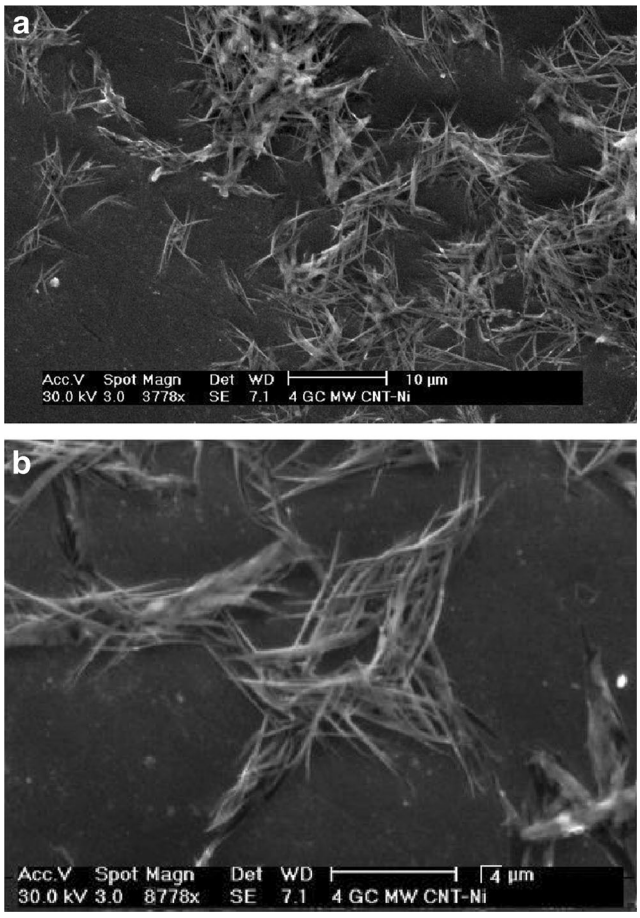

Fig. 2 **a** Low magnification picture and **b** detailed scanning electron micrograph of an activated GC/MWCNT-Ni surface electrode. Electrodeposition conditions of nickel species were performed as reported in the "Electrode preparation" section

XPS characterization of the activated GC/MWCNTs and GC/MWCNT-Ni

XPS was used to define the surface chemical composition of the GC/MWCNT-Ni electrode prepared by the pulsed electrodeposition procedure. Throughout this study, the C1s, O1s, and Ni 2p core level spectra were collected and analyzed. Typical XP spectra of the C1s region of an activated and non-activated GC/MWCNT electrode are shown in Fig. 3a, b, respectively. The C1s peak exhibits a pronounced asymmetric tailing toward higher binding energy (BE) values. The tail arises partly from the intrinsic asymmetry of the C1s signal [41] and partially from contributes arising from oxygen-containing functional groups such as alcohol (C–OH), ketone (C=O), and carboxylic species (COOH) and additional peaks derived from plasmon satellite and carbonate species [41, 42]. In good agreement with the literature, the peaks at 286.0 ± 0.2, 287.4 ± 0.2, 289.0 ± 0.2, and 290.3 ± 0.2 eV can be assigned to C–OH, C=O, COOH, and CO_3^- species, respectively. It is interesting to underline that the C1s signal from the activated GC/MWCNT substrate shows an intense contribute at about 289.0 ± 0.2 eV, ascribed to carboxyl species. This last signal, ascribed to the carboxyl group, represents the main product of the electrochemical activation of the multi-walled nanotubes. Figure 4 shows the XP spectra of the Ni 2p detailed region. Although the electrochemical redox transition of the Ni(II)/Ni(III) (see Fig. 1) is characterized by high intensities of the peak currents, the Ni 2p spectral region shows always very low intensity of the photoelectron signals. This behavior seems to further support the hypothesis that a significant amount of nickel species can be deposited inside multi-walled nanotubes rather than the outer surface of the carbon bundles (see Fig. 2). In this study, the main signal of the Ni $2p_{3/2}$ could be deconvoluted into two components at about 856.2 ± 0.2 and 858.0 ± 0.2 eV, assigned to $Ni(OH)_2$ and NiOOH species, respectively [36, 41–43]. The curve fitting of the O1s signal (not shown) indicates that there are usually up to three component peaks with BE comprised between 529

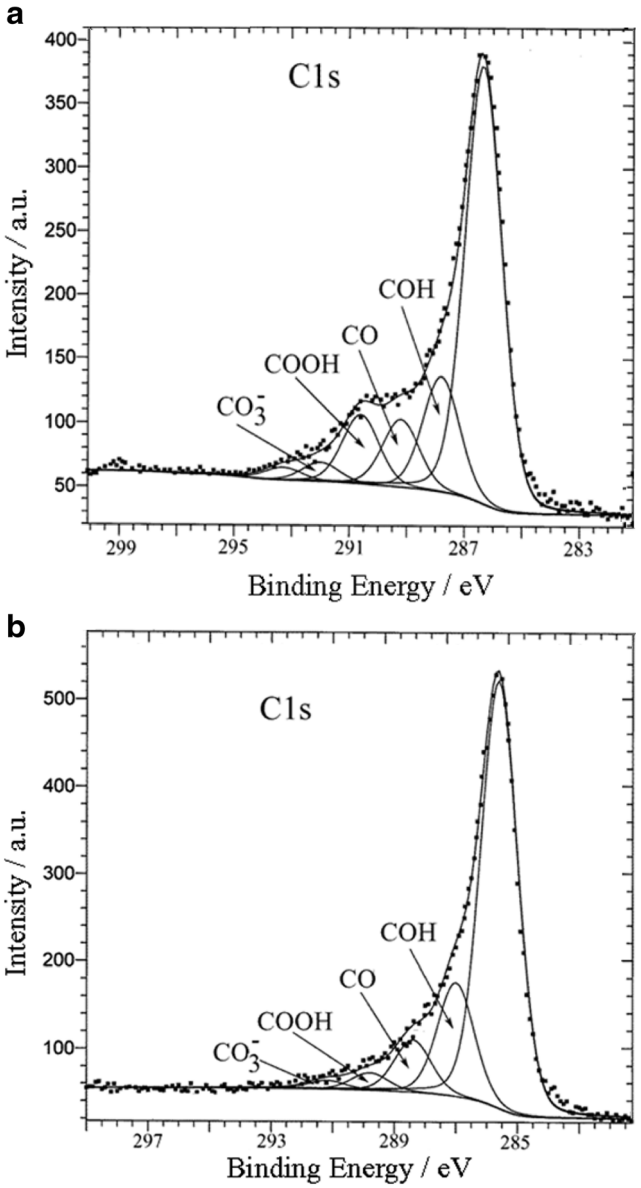

Fig. 3 The XPS-detailed C1s region of the activated GC/MWCNT electrode (**a**) and not activated GC/MWCNT substrate electrode (**b**). The electrochemical activation of the electrode substrate was carried out as reported in the "Electrode preparation" section

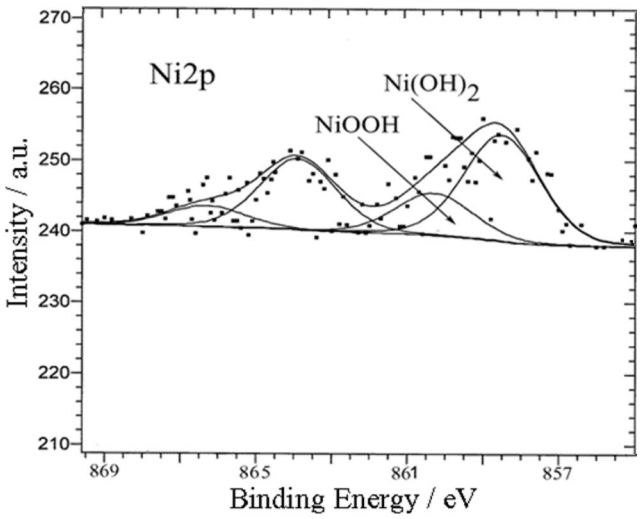

Fig. 4 The XPS-detailed Ni 2p region of the activated GC/MWCNT-Ni electrode

In order to provide a better understanding of the surface nature of the GC/MWCNT-Ni, a comparison between the C1s, O1s, and Ni 2p detailed regions was carried out. The relevant results are summarized in Table 3. As can be seen, it is possible to make some considerations:

i) The electrochemical activation of the MWCNTs in 0.5 M K_2SO_4 solution induces a significant increase in the atomic ratio between the O1s and C1s signals. This result supports the hypothesis that the electrochemical activation introduces surface groups with oxidized species (i.e., C–OH, C=O, and COOH).

ii) The electrochemical activation induces a sensible increase of the carboxyl content (COOH) on the total carbonaceous species present on the electrode surface. The atomic ratio $C1s_{(COOH)}/C1s_{Total}$ reaches the maximum value of 0.1 only after electrochemical activation of the MWCNTs.

and 534 eV, tentatively assigned to hydroxide species, C=O, COOH, adsorbed oxygen and/or water, etc. [36, 41–43]. The exact assignment of the O1s contributes is complex and ambiguous owing to uncertainty in the BE values of the various oxygen species. However, in this study, we consider, in view of the comparison between the different electrode surfaces, only the total area of the O1s signal. Consequently, the exact assignment of the specific peaks under the O1s signal is not essential. The substantial absence of the N1s photoelectron signal on the electrode surface suggests that the EDTA ligand was not incorporated into the nickel oxide lattice of the GC/MWCNT-Ni electrode.

These XPS results obtained here, although not conclusive, show that the electrochemical activation of the MWCNTs induces the effective formation of oxygen-containing functional groups. Thus, it can be hypothesized that the surface interaction between oxidized functional groups and adsorbed complexes species of EDTA-Ni plays an important role on the overall electrodeposition process of nickel oxide on the activated GC/MWCNTs. In support of this assumption, the formation of some carbonyl-metal bridges was invoked during some electrodeposition processes of cobalt and platinum species from alkaline and acid medium, respectively [31, 44].

Table 3 XPS results relevant to the nickel pulsed electrodeposition on the GC/MWCNT substrate from alkaline solutions containing Ni(II) and EDTA complex species

Sample	Ni(II)/Ni(III)	O1s/C1s	$C1s_{ox}/C1s_{Total}$	$C1s_{(COOH)}/C1s_{Total}$
GC/MWCNT-Ni	3.3	0.54	0.5	0.1
GC/MWCNT	–	0.4	0.4	0.1
GC/MWCNT*[a]	–	0.17	0.3	>0.04
GC	–	0.35	0.4	0.1
GC-Ni	3.0	0.48	0.4	0.1

The nickel was deposited on the electrochemically activated GC/MWCNT electrode using a depositing solution containing 2.0 M NaOH plus 5 mM $Ni(NO_3)_2$ and 5.0 mM EDTA. The pulsed conditions were $E_1 = -0.2$ V vs. SCE (0.3 s) and $E_2 = 0.7$ V vs. SCE (0.03 s) for the electrodeposition time of 100 s. The $C1s_{ox}/C1s_{Total}$ represents the atomic ratios between the oxidized contribution under the C1s and the total C1s XP signals. The $C1s_{(COOH)}/C1s_{Total}$ represents the atomic ratios between the contribution at 289.0 ± 0.2 eV and the total C1s photoelectron signal

[a] The electrode substrate not electrochemically activated. The electrochemical activation procedure of the GC or GC/MWCNTs was reported in the "Electrode preparation" section

Amperometric characterization of the GC/MWCNT-Ni electrode toward the electrooxidation of aliphatic alcohols

Representative cyclic voltammograms obtained at the GC/MWCNT-Ni-modified electrode in 1.0 M NaOH solution and containing increasing concentrations of ethanol are reported in Fig. 5. It can be readily seen that the modified electrode shows excellent electrocatalytic activity toward alcohol oxidation at potentials higher than 0.45 V vs. SCE. The currents increased linearly with analyte concentration until 40–45 mM with correlation coefficients greater than 0.99. It has been widely accepted that NiOOH species acts as powerful active electrocatalyst for the oxidation of several organic compounds [21, 45]. However, the electrooxidation of the alcohol reduces the surface amount of NiOOH species, and this explains the significant decrease in the magnitude of the cathodic peak I_c after analyte addition. A similar voltammetric profile was observed for other tested aliphatic alcohols; however, the intensities of the oxidation currents decrease in the following order: methanol > ethanol > propanol ≈ butanol, suggesting the onset of some steric hindrance on the overall reaction mechanism of the alcohol oxidation process.

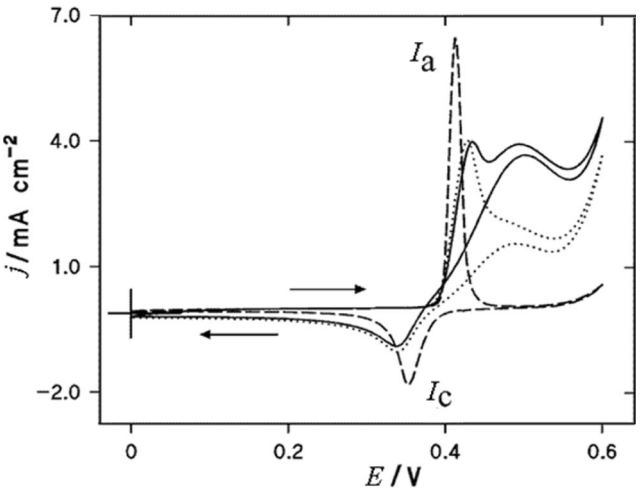

Fig. 5 Voltammograms (fifth cycle) obtained on the activated GC/MWCNT-Ni-modified electrode in 1.0 M NaOH solution (*dashed curve*), plus 16 mM ethanol (*dotted curve*), and 32 mM ethanol (*solid curve*). The GC/MWCNT-Ni-modified electrode was prepared as in Fig. 2; scan rate, 50 mV s^{-1}

In order to evaluate the electrocatalytic performance of the studied GC/MWCNT-Ni-modified electrode, we have compared its electrochemical behavior to pure nickel electrode (nickel bare electrode) for the electrooxidation of 20 mM ethanol under chronoamperometric measurements. The optimized chronoamperometry used here employs a continuous repetition of two potentials, fixed at 0.3 and 0.5 V vs. SCE, each for 10 s. The relevant performance of the GC/MWCNT-Ni and nickel bare electrode is shown in Fig. 6a, b, respectively. As can be seen, by comparing Fig. 6a and Fig. 6b, some important considerations can be made:

i) In the presence of 20 mM ethanol, the GC/MWCNT-Ni-modified electrode shows a charge associated to the electrooxidation process that is significantly greater than that observed on the nickel bare electrode. The charge related to the oxidation process on the GC/MWCNT-Ni represents about 150 % of the relevant background charge measured in the absence of ethanol, while on the nickel bare electrode, the corresponding charge represents only 40 %.

ii) After repetitive pulses of potentials between 0.3 and 0.5 V vs. SCE, the catalytic efficiency of the GC/MWCNT-Ni electrode toward ethanol electrooxidation remains practically unchanged indicating a good electrochemical and mechanical stability of the catalyst.

iii) In the presence of ethanol, the oxidation currents observed during the application of each pulse potential

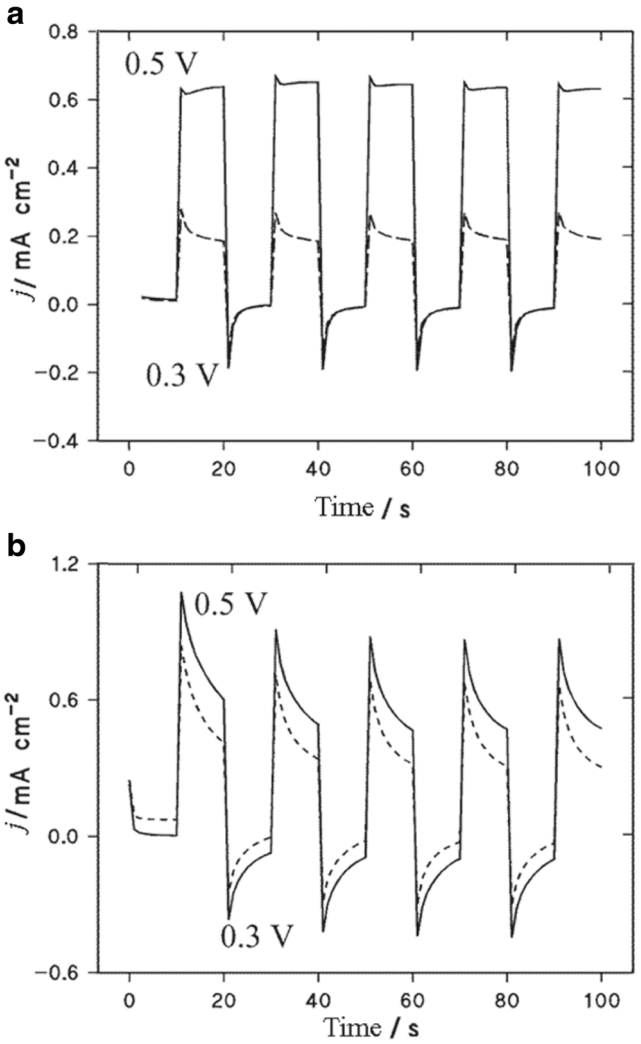

Fig. 6 Chronoamperometric measurements obtained using a continuous repetition of two applied potentials, fixed at 0.3 and 0.5 V (vs. SCE), each for 10 s, and alkaline stirred solutions (*magnetic bar* at about 200 rpm). **a** The GC/MWCNT-Ni-modified electrode in 1.0 M NaOH solution (*dashed curve*), plus 20 mM ethanol (*solid curve*). **b** The nickel bare electrode in 1.0 M NaOH solution (*dashed curve*), plus 20 mM ethanol (*solid curve*). The GC/MWCNT-Ni-modified electrode was prepared as in Fig. 2

decreases slightly when the GC/MWCNT-Ni electrode was used. During 10 s of pulse duration, a decrease of oxidation current of about 4 % on the GC/MWCNT-Ni was observed, while on the corresponding nickel bare electrode, the oxidation currents decrease by about 46 %.

Thus, the proposed GC/MWCNT-Ni-modified electrode shows very interesting catalytic activity with excellent temporal stability toward electrooxidation of some aliphatic alcohols in alkaline medium, confirming its potential performance in electroanalytical applications.

Conclusions

We have prepared, through pulsed electrodeposition procedure, a modified GC electrode based on Ni oxyhydroxide particles dispersed within multi-walled carbon nanotubes from alkaline solutions containing Ni-EDTA complex species. The influence of pulse amplitude, [EDTA]/[Ni(II)] concentration ratio, and [OH^-] on the rate of the nickel deposition process was evaluated. In particular, the effect of the electrochemical activation of the MWCNTs on the nickel deposition efficiency was evaluated and discussed. The chemical surface nature of the GC/MWCNT-Ni-modified electrode was studied through the curve-fitting analysis of the C1s, O1s, and Ni 2p detailed regions. These XPS results show that the electrochemical activation of the MWCNTs induces the effective formation of carboxyl surface groups (COO^-), which play an essential role on the electrodeposition process of nickel oxyhydroxide species. The surface-modified electrode based on MWCNTs containing dispersed nickel particles shows good electrocatalytic properties toward electrooxidation of some aliphatic alcohols in alkaline medium.

References

1. Lipkowski J, Ross PN (1994) Eds, electrochemistry of novel materials: frontiers of electrochemistry. VCH Publishers Inc, Weinheim
2. Bunshah RF (1994) Handbook of deposition technologies for films and coating: science, technology and applications, 2nd edn. Park Ridge, Noyes Publishing
3. Lue JT (2001) A review of characterization and physical property studies of metallic nanoparticles. J Phys Chem Solids 62:1599–1612
4. Campbell FW, Compton RG (2010) The use of nanoparticles in electroanalysis: an updated review. Anal Bioanal Chem 396:241–259
5. Wu MS, Huang YA, Yang CH, Jow JJ (2007) Electrodeposition of nanoporous nickel oxide film for electrochemical capacitors. Int J Hydrog Energy 32:4153–4159
6. Li Y, Ye K, Cheng K, Yin J, Cao D, Wang G (2015) Electrodeposition of nickel sulfide on graphene-covered make-up cotton as a flexible electrode material for high-performance supercapacitors. J Power Sources 274:943–950
7. Mc Breen J, White RE, Bockris JO, Conway BE (1990) Modern aspects of electrochemistry Eds. Plenum Press, New York
8. Kamath PV, Dixit M, Indira L, Shukla AK, Kumar VG, Munichandraiah N (1994) Stabilized α-$Ni(OH)_2$ as electrode material for alkaline secondary cells. J Electrochem Soc 141:2956–2959
9. Freitas MBJG (2001) Nickel hydroxide powder for NiOOH/$Ni(OH)_2$ electrodes of the alkaline batteries. J Power Sources 93:163–173
10. Kohler U, Antonius C, Bauerlein PJ (2004) Advances in alkaline batteries. Power Sources 127:45–52
11. Sierczynska A, Lota K, Lota G (2010) Effects of addition of different carbon materials on the electrochemical performance of nickel hydroxide electrode. J Power Sources 195:7511–7516
12. Schulze M, Gülzow E, Steinhilber G (2001) Activation of nickel-anodes for alkaline fuel cells. Appl Surf Sci 179:251–256

13. Schulze M, Gülzow E (2004) Degradation of nickel anodes in alkaline fuel cells. J Power Sources 127:252–263
14. Wu H, Wexler D, Wang G (2009) Pt_xNi alloy nanoparticles as cathode catalyst for PEM fuel cells with enhanced catalytic activity. J Alloys Compd 488:195–198
15. Ghasemi M, Wan Daud WR, Rahimnejad M, Rezayi M, Fatemi A, Jafari Y, Somalu MR, Manzour A (2013) Copper-phthalocyanine and nickel nanoparticles as novel cathode catalyst in microbial fuel cells. Int J Hydrog Energy 38:9533–9540
16. Gunjakar JL, More AM, Lokhande CD (2008) Chemical deposition of nanocrystalline nickel oxide from urea containing bath and its use in liquefied petroleum gas sensor. Sensors Actuators B Chem 131:356–361
17. Vidotti M, Cerri CD, Carvalhal RF, Dias JC, Mendes RK, de Torresi SI C, LT K (2009) Nickel hydroxide electrodes as amperometric detectors for carbohydrates in flow injection analysis and liquid chromatography. J Electroanal Chem 636:18–23
18. Sattarahmady N, Heli H, Dehdari Vais R (2013) An electrochemical acetylcholine sensor based on lichen-like nickel oxide nanostructure. Biosens Bioelectron 48:197–202
19. Kung CW, Cheng YH, Ho KC (2014) Single layer of nickel hydroxide nanoparticles covered on a porous Ni foam and its application for highly sensitive non-enzymatic glucose sensor. Sensors Actuators B Chem 204:159–166
20. Pissinis DE, Sereno LE, Marioli JM (2014) Non-enzymatic sensing of carbohydrates using a nickel-chromium alloy electrode. Sensors Actuators B Chem 193:46–52
21. Casella IG, Cataldi TRI, Salvi AM, Desimoni E (1993) Electrocatalytic oxidation and liquid chromatographic detection of aliphatic alcohols at a nickel-based glassy carbon modified electrode. Anal Chem 65:3143–3150
22. Casella IG, Rosa S, Desimoni E (1998) Electrooxidation of aliphatic amines and their amperometric detection in flow injection and liquid chromatography at a nickel-based glassy carbon electrode. Electroanalysis 10:1005–1009
23. Casella IG, Guascito MR, Sannazzaro MG (1999) Voltammetric and XPS investigations of nickel hydroxide electrochemically dispersed on gold surface electrodes. J Electroanal Chem 462:202–210
24. Casella IG, Gatta M, Cataldi TRI (2000) Amperometric determination of underivatized amino acids at a nickel-modified gold electrode by anion-exchange chromatography. J Chromatogr A 878:57–67
25. Zhao Q, Gan Z, Zhuang Q (2002) Electrochemical sensors based on carbon nanotubes. Electroanalysis 14:1609–1613
26. Tortorich RP, Song E, Choi JW (2014) Inkjet-printed carbon nanotube electrodes with low sheet resistance for electrochemical sensor applications. J Electrochem Soc 161:B3044–B3048
27. Li L, Lafdi K (2008) Nickel modification of carbon nanotubes grown on graphite for electrochemical sensors. Sensors Actuators B Chem 132:202–208
28. Chen YS, Huang JH (2010) Arrayed CNT-Ni nanocomposites grown directly on Si substrate for amperometric detection of ethanol. Biosens Bioelectron 26:207–212
29. Sun A, Zheng J, Sheng Q (2012) A highly sensitive non-enzymatic glucose sensor based on nickel and multi-walled carbon nanotubes nanohybrid films fabricated by one-step co-electrodeposition in ionic liquids. Electrochim Acta 65:64–69
30. Bjelica LJ, Jovanovic LS (1992) Activation of glassy carbon electrode in aqueous and non-aqueous media. Electrochim Acta 37:371–372
31. Guo DJ, Li HL (2004) High despersion and electrocatalytic properties of Pt nanoparticles on SWNT bundles. J Electroanal Chem 573:197–202
32. Sitko R, Zawisza B, Malicka E (2012) Modification of carbon nanotubes for preconcentration, separation and determination of trace-metal ions. Trends Anal Chem 37:22–31
33. Bernard MC, Bernard P, Keddam M, Senyarich S, Takenouti H (1996) Characterisation of new nickel hydroxides during the transormation of α $Ni(OH)_2$ to β $Ni(OH)_2$ by ageing. Electrochim Acta 41:91–93
34. Sac-Epée N, Palacìn MR, Delahaye-Vidal A, Chabre Y, Tarâscon JM (1998) Evidence for direct γ NiOOH ↔ β Ni(OH)2 transitions during electrochemical cycling of the nickel hydroxide electrode. J Electrochem Soc 145:1434–1441
35. Van der Ven A, Morgan D, Meng YS, Ceder G (2006) Phase stability of nickel hydroxides and oxyhydroxides. J Electrochem Soc 153:A210–A215
36. Casella IG, Spera R (2005) Electrochemical deposition of nickel and nickel-thallium composite oxides films from EDTA alkaline solutions. J Electroanal Chem 578:55–62
37. Schlesinger M, Paunovic M (2010) Eds, Modern Electroplating, 5th Ed, Wiley & Sons Inc.
38. Visscher W, Barendrecht E (1980) Absorption of hydrogen in reduced nickel oxide. J Appl Electrochem 10:269–274
39. Nhut JM, Pesant L, Tessonnier JP, Winné G, Guille J, Pham-Huu C, Ledoux MJ (2003) Mesoporous carbon nanotubes for use as support in catalysis and as nanosized reactors for one-dimensional inorganic material synthesis. Appl Catal A 254:345–363
40. Tessonnier JP, Pesant L, Ehret G, Ledoux MJ, Pham-Huu C (2005) Pd nanoparticles introduced inside multi-walled carbon nanotubes for selective hydrogenation of cinnamaldehyde into hydrocinnamaldehyde. Appl Catal A 288:203–210
41. Wagner CD, Riggs WM, Davis LE, Moulder JF, Mouilenberg GE (1978) Handbook of X-ray photoelectron spectroscopy. Perkin-Elmer Corporation, Eden Prairie, Minnesota
42. Desimoni E, Casella IG, Morone A, Salvi AM (1990) XPS determination of oxygen-containing functional groups on carbon-fibre surfaces and the cleaning of these surfaces. Surf Interface Anal 15:627–634 and literature cited therein
43. Luo PF, Kuwana T, Paul DK, Sherwood PMA (1996) Electrochemical and XPS study of the nicke-titanium electrode surface. Anal Chem 68:3330–3337
44. Casella IG, MR G (1999) Anodic electrodeposition of conducting cobalt oxyhydroxide films on a gold surface. J Electroanal Chem 476:54–63
45. Fleishman M, Korinek K, Pletcher D (1971) The oxidation of organic compounds at a nickel anode in alkaline solution. J Electroanal Chem 31:39–49